Supplemental Information for Nature of the Magnetic Interactions in Sr_3NiIrO_6

Turan Birol
Department of Physics and Astronomy, Rutgers University, Piscataway, New Jersey 08854, USA and
Department of Chemical Engineering and Materials Science,
University of Minnesota, Minneapolis, Minnesota 55455, USA

Kristjan Haule and David Vanderbilt
Department of Physics and Astronomy, Rutgers University, Piscataway, New Jersey 08854, USA
(Dated: October 7, 2018)

METHODS

First principles density functional theory (DFT) calculations were performed using Vienna Ab Initio Simulation Package (VASP), which uses the projector augmented wave method [1–4]. PBEsol exchange correlation functional [5] is used in conjunction with the DFT+U as introduced by Dudarev et al. [6]. The value of U has been chosen as $U_{\mathrm{Ir}} = 2$ eV and $U_{\mathrm{Ni}} = 4$ eV for Ir and Ni respectively. This choice of U gives the magnetic (spin + orbital) moments of $\mu_{\mathrm{Ir}} \sim 0.6\mu_B$ and $\mu_{\mathrm{Ni}} \sim 1.8\mu_B$, which are in reasonable agreement with $\mu_{\mathrm{Ir}} \sim 0.5\mu_B$ and $\mu_{\mathrm{Ni}} \sim 1.5\mu_B$ observed in experiment [7]. Small variations in the values of U's give rise to quantitative changes, but the magnetic ground state does not change. A plane-wave basis cutoff energy of 500 eV, and a $8 \times 8 \times 8$ k-point grid for the 22 atom primitive unit cell, which corresponds to one k-point per $\sim 0.02\ 2\pi/\text{Å}$, is found to provide good convergence of the electronic properties. Spin-orbit coupling is taken into account in all calculations unless otherwise stated.

CRYSTAL AND MAGNETIC STRUCTURE

Sr_3NiIrO_6 crystallizes in the K_4CdCl_6 structure, which consists of parallel one-dimensional chains of alternating, face sharing NiO_6 and IrO_6 polyhedra (Fig. 1a and Table I) [8, 9]. Its space group is trigonal $R\bar{3}c$, and the 3-fold rotation axis passes through the cations, parallel to the chains, along the crystallographic c axis (Fig. 1b). There are three 2-fold rotation axes perpendicular to the 3-fold one, passing through the Ni cations, and inversion centers on the Ir cations. Ir ions are surrounded by oxygen octahedra whereas Ni ions are at the center of oxygen trigonal prisms. The octahedra and prisms are face sharing with each other, which enables strong direct cation - cation direct interactions [10].

ORBITAL CONFIGURATIONS OF Ir^{4+} AND Ni^{2+}

The site symmetries of the Ir and Ni cations in Sr_3NiIrO_6 are $\bar{3}$ and 32 respectively, as shown in Table I and Fig. 1. Both of them have their d orbitals split into 2+2+1. This splitting can be considered the result of coexisting cubic and trigonal crystal fields on each ion. The ratio of the trigonal to cubic crystal field strengths is expected to be larger for the Ni ion, because it is on a trigonal prismatic site, whereas Ir is on a (only slightly distorted) octahedral site [11, 12]. Using a cubic point group as reference, we can consider a higher energy e_g-like doublet, and three lower energy t_{2g}-like orbitals which are split into 2+1 [13]. (Henceforth, we omit the '-like' suffix and simply refer to e_g and t_{2g} states.) The relative energies of the t_{2g} singlet and the doublet is not determined by symmetry. The t_{2g} doublet transforms as the same irrep as the e_g doublet, and hence can mix with it. (In the following, we ignore this mixing, which is not important for the current discussion.) A convenient choice of cartesian basis is one with the $\hat{z}$ along the crys-

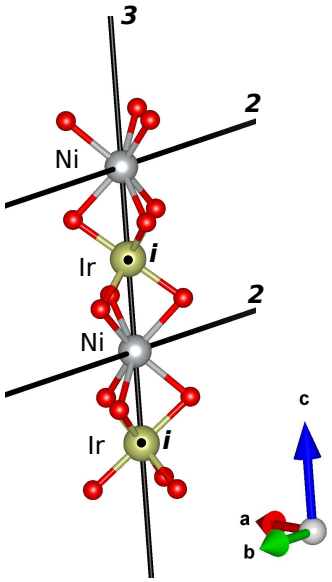

FIG. 1. (Color Online) Crystal structure of Sr_3NiIrO_6 consists of one-dimensional chains along the c axis that consist of face-sharing NiO_6 and IrO_6 polyhedra. There is a 3-fold rotational symmetry axis along each chain, as well as 2-fold axes passing through the Ni sites, and inversion centers on the Ir sites.

Space Group:		$R\bar{3}c$
Space Group Number:		167
Lattice constants:		$a = 9.578$ Å
		$c = 11.132$ Å
Ion	Wyckoff Position	Site Symmetry
Sr	18e	1
Ni	6a	32
Ir	6b	$\bar{3}$
O	36f	1

TABLE I. Details of the crystal structure of Sr_3NiIrO_6. Crystal structure data taken from Nguyen et al. [9].

tallographic c axis (chain direction), and the $\hat{x}$ and $\hat{y}$ on the a-b plane (Fig. 1c). With this axis choice, the three t_{2g} orbitals can be written as

$$|A\rangle = |3z^2 - r^2\rangle \tag{1}$$

$$|E^+\rangle = -\frac{i}{\sqrt{3}}|xy\rangle + \frac{i}{\sqrt{6}}|xz\rangle + \frac{1}{\sqrt{6}}|yz\rangle - \frac{1}{\sqrt{3}}|x^2-y^2\rangle \tag{2}$$

$$|E^-\rangle = +\frac{i}{\sqrt{3}}|xy\rangle - \frac{i}{\sqrt{6}}|xz\rangle + \frac{1}{\sqrt{6}}|yz\rangle - \frac{1}{\sqrt{3}}|x^2-y^2\rangle \tag{3}$$

in terms of the cubic harmonics.

Under a cubic crystal field, the spin-orbit coupling is known to mix and split the t_{2g} cubic harmonic orbitals to give rise to the higher energy pair of so called $J_{\text{eff}} = 1/2$ states. For an octahedron that has corners along the cartesian axes, these $|J_{1/2}, \uparrow\rangle$ and $|J_{1/2}, \downarrow\rangle$ states are often written as

$$|J_{1/2}, \uparrow\rangle = \frac{1}{\sqrt{3}}\left(-|xy, \downarrow\rangle - i|xz, \uparrow\rangle + |yz, \uparrow\rangle\right) \tag{4}$$

and

$$|J_{1/2}, \downarrow\rangle = \frac{1}{\sqrt{3}}\left(+|xy, \uparrow\rangle + i|xz, \downarrow\rangle + |yz, \downarrow\rangle\right). \tag{5}$$

These states exhibit spin-orbital entanglement in the sense that the $|xy\rangle$ part has an opposite spin to the rest. Similarly, with our choice of axes for the Ir atom (where the corners of the octahedra are along the $\langle 111\rangle$) and the trigonal crystal field, diagonalizing the $\vec{L}\cdot\vec{S}$ operator in the t_{2g} subspace gives the $J_{\text{eff}} = 1/2$ states as

$$|J_{1/2}, \uparrow\rangle = \frac{1}{\sqrt{|\gamma|^2+2}}\left(i\gamma|A, \downarrow\rangle + \sqrt{2}|E^+, \uparrow\rangle\right) \tag{6}$$

and

$$|J_{1/2}, \downarrow\rangle = \frac{1}{\sqrt{|\gamma|^2+2}}\left(i\gamma|A, \uparrow\rangle + \sqrt{2}|E^-, \downarrow\rangle\right) \tag{7}$$

where we ignored the mixing with the e_g orbitals. Here, the magnetic moments of either state are along the $\hat{z}$ direction, which is the crystallographic c axis. In the absence of the trigonal crystal field, $\gamma = 1$, and these states have exactly $33.\bar{3}\%$ $|A\rangle = |3z^2 - r^2\rangle$ character with spin opposite to the rest of the state. This is very close to the first principles result of 36% $|3z^2 - r^2\rangle$ character for the t_{2g} hole on Ir, showing that the trigonal field is not strong enough to significantly change the orbital and spin characteristics of the Ir ion.

DENSITY OF STATES OF NI

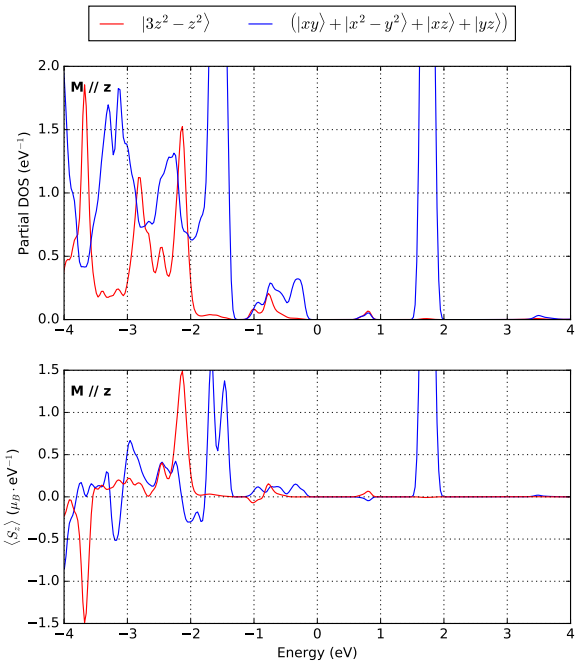

FIG. 2. (Color Online) (a) Densities of states of the Ni ion projected onto the d orbitals in the FiM state with magnetic moments along the z axis (magnetic ground state). (b) Energy resolved expectation value of the z component of spin, $\langle S_z\rangle$ for the d orbitals of the Ni ion in the FiM state with magnetic moments along the z axis.

The Ni^{2+} cation has 8 electrons, and its t_{2g}-like orbitals are completely filled. The unoccupied DOS between 1.5 and 2.0 eV's is that of the two holes in the half-filled e_g-like orbitals, which have no $|3z^2 - r^2\rangle$ character as expected.

MAGNON SPECTRUM

In this section, we calculate the magnon spectrum of Sr_3NiIrO_6 using the model

$$E = \sum_n \left[J_\parallel \left(M^{Ir}_{n,z}(M^{Ni}_{n,z} + M^{Ni}_{n+1,z}) \right) + J_\perp \left(M^{Ir}_{n,x}(M^{Ni}_{n,x} + M^{Ni}_{n+1,x}) + M^{Ir}_{n,y}(M^{Ni}_{n,y} + M^{Ni}_{n+1,y}) \right) \right] \tag{8}$$

with parameters from first principles to show that a model without single ion anisotropy is sufficient to explain the large gap in the magnon spectrum.

We introduce new operators, $\hat{Q}$ and $\hat{R}$, for the pseudospins of the two ions:

$$M^{Ni}_{n,z} = \hat{Q}^z_n \tag{9}$$

$$M^{Ni}_{n,x} = \frac{1}{2}\left(\hat{Q}^+_n + \hat{Q}^-_n\right) = \hat{Q}_x \tag{10}$$

$$M^{Ni}_{n,y} = \frac{1}{2i}\left(\hat{Q}^+_n - \hat{Q}^-_n\right) = \hat{Q}_y \tag{11}$$

$$M^{Ir}_{n,z} = -\hat{R}^z_n \tag{12}$$

$$M^{Ir}_{n,x} = -\frac{1}{2}\left(\hat{R}^+_n + \hat{R}^-_n\right) = -\hat{R}_x \tag{13}$$

$$M^{Ir}_{n,y} = \frac{1}{2i}\left(\hat{R}^+_n - \hat{R}^-_n\right) = \hat{R}_y \tag{14}$$

Both $\hat{Q}$ and $\hat{R}$ satisfy the usual commutation relations such as $[\hat{Q}_i, \hat{Q}_j] = i\hbar\varepsilon_{ijk}\hat{Q}_k$.

The magnetic hamiltonian takes the form:

$$\mathcal{H} = \sum_n \left\{ -J_\parallel \left[\hat{Q}^z_n(\hat{R}^z_n + \hat{R}^z_{n+1}) \right] + J_\perp \left[\hat{Q}^x_n(\hat{R}^x_n + \hat{R}^x_{n+1}) - \hat{Q}^y_n(\hat{R}^y_n + \hat{R}^y_{n+1}) \right] \right\} \tag{15}$$

We now make the approximations that $\hat{Q}^z_n \hat{R}^\mp_m = \mu_{\rm Ni}\hat{R}^\mp_m$ and $\hat{R}^z_n \hat{Q}^\mp_m = \mu_{\rm Ir}\hat{Q}^\mp_m$ This approximation is valid in the ordered state for small amplitude of excitations [14, 15]. It gives

$$\frac{1}{\hbar}[\hat{R}^-_n, \mathcal{H}] = -2J_\parallel \mu_{\rm Ni}\hat{R}^-_n - J_\perp \mu_{\rm Ir}(\hat{Q}^+_n + \hat{Q}^+_{n-1}) \tag{16}$$

$$\frac{1}{\hbar}[\hat{Q}^+_n, \mathcal{H}] = +2J_\parallel \mu_{\rm Ir}\hat{Q}^+_n + J_\perp \mu_{\rm Ni}(\hat{R}^-_n + \hat{R}^-_{n+1}) \tag{17}$$

Introducing the Fourier transformed operators

$$\hat{Q}^+_q = \sum_n e^{-iqn}\hat{Q}^+_n \tag{18}$$

$$\hat{R}^-_q = \sum_n e^{-iqn}\hat{R}^-_n \tag{19}$$

we obtain their time evolution as

$$i\frac{\partial}{\partial t}\hat{R}^-_q = \frac{1}{\hbar}[\mathcal{H}, \hat{R}^-_q] = J_\perp \mu_{\rm Ir}(1 + e^{-iqc})\hat{Q}^+_q + 2J_\parallel \mu_{\rm Ni}\hat{R}^-_q \tag{20}$$

and

$$i\frac{\partial}{\partial t}\hat{Q}^+_q = \frac{1}{\hbar}[\mathcal{H}, \hat{Q}^+_q] = -J_\perp \mu_{\rm Ni}(1 + e^{+iqc})\hat{R}^-_q - 2J_\parallel \mu_{\rm Ir}\hat{Q}^+_q \tag{21}$$

where c is the lattice constant along the [001] direction and q is the wavevector along the same axis. We can write these two equations as

$$i\frac{\partial}{\partial t}\begin{pmatrix} \hat{Q}^+_q \\ \hat{R}^-_q \end{pmatrix} = M \begin{pmatrix} \hat{Q}^+_q \\ \hat{R}^-_q \end{pmatrix} \tag{22}$$

$$M = \begin{pmatrix} -2J_\parallel \mu_{\rm Ir} & -J_\perp(1 + e^{iqc})\mu_{\rm Ni} \\ J_\perp(1 + e^{-iqc})\mu_{\rm Ir} & 2J_\parallel \mu_{\rm Ni} \end{pmatrix} \tag{23}$$

We define the magnon creation/annihilation operators for the two branches via a matrix K that diagonalizes M:

$$\begin{pmatrix} \hat{Q}^+_q \\ \hat{R}^-_q \end{pmatrix} = K \begin{pmatrix} \hat{\alpha}_q \\ \hat{\beta}^\dagger_q \end{pmatrix} \tag{24}$$

which leads to

$$\begin{pmatrix} -\omega_{q,\alpha}\hat{\alpha}^\dagger_q \\ \omega_{q,\beta}\hat{\beta}_q \end{pmatrix} = K^{-1}MK \begin{pmatrix} \hat{\alpha}^\dagger_q \\ \hat{\beta}_q \end{pmatrix} \tag{25}$$

Now $\mathcal{H} = \sum_q \left[\omega_{q,\alpha}\hat{\alpha}^\dagger_q\hat{\alpha}_q + \omega_{q,\beta}\hat{\beta}^\dagger_q\hat{\beta}_q \right]$. We define the components of K as

$$K = \begin{pmatrix} u_q & v^*_q \\ \sqrt{\sigma}v_q & \sqrt{\sigma}u^*_q \end{pmatrix} \tag{26}$$

so that

$$K^{-1} = \begin{pmatrix} u^*_q & -v^*_q/\sqrt{\sigma} \\ -v_q & u_q/\sqrt{\sigma} \end{pmatrix} \tag{27}$$

where we have imposed $|u|^2 - |v|^2 = 1$. The offdiagonal elements of $K^{-1}MK$ are set to zero to solve for u and v, and the diagonal elements (one of which is multiplied by -1 gives the energies of the two magnon modes as

$$\omega_{\alpha,q} = J_{\parallel}(\mu_{\rm Ni} - \mu_{\rm Ir}) + \sqrt{J_{\parallel}^2(\mu_{\rm Ni} + \mu_{\rm Ir})^2 - 2J_{\perp}^2\mu_{\rm Ni}\mu_{\rm Ir}(1 + \cos qc)} \tag{28}$$

$$\omega_{\beta,q} = -J_{\parallel}(\mu_{\rm Ni} - \mu_{\rm Ir}) + \sqrt{J_{\parallel}^2(\mu_{\rm Ni} + \mu_{\rm Ir})^2 - 2J_{\perp}^2\mu_{\rm Ni}\mu_{\rm Ir}(1 + \cos qc)} \tag{29}$$

According to these expressions, the ratio of the bandwidth to the gap is $\sim J_{\perp}^2/J_{\parallel}^2$. In other words, they readily reproduce the gap being much larger than the dispersion. The magnon spectra, plotted in Fig. 4(c) in the main text, are consistent with the experimental observations that there is a large gap both between the two magnon branches, and with the lower branch and zero energy. The quantitative agreement is not perfect, for example, the upper branch is experimentally observed to be around 90 meV [16]. Fine tuning the U parameters in our DFT+U calculations can provide better agreement.

We note that the sign of $J_{\perp}$ does not enter to the energy expression for the magnons, so the magnon spectra do not provide any evidence for the sign difference between $J_{\parallel}$ and $J_{\perp}$. However, the relative intensities of the two branches can carry information about this sign difference. At the Γ point ($q = 0$), the components of the matrix K that diagonalizes M give

$$\frac{u_{q=0}}{v_{q=0}} = -\frac{J_{\parallel}(1+\sigma)}{2J_{\perp}\sqrt{\sigma}}\left(1 \pm \sqrt{1 - \frac{\sigma|2J_{\perp}|^2}{(J_{\parallel})^2(1+\sigma)^2}}\right) \tag{30}$$

(We have defined $\sigma = \mu_{\rm Ir}/\mu_{\rm Ni}$, and only the root with the + sign gives $u > v$.) Plugging in $J_{\parallel} \sim -2J_{\perp}$ and $\mu_{\rm Ni} \sim 3\mu_{\rm Ni}$, we get $u \sim 4v$. This means that the lower lying β branch is dominated by Ni, whereas the α branch is dominated by Ir, consistent with the fact that RIXS does not observe the lower branch [16, 17].

Equation 30 indicates that the relative sign of u and v depends on the sign of $J_{\perp}$. This sign difference enters the expression of the cross sections for creation of a magnon with q

$$\left(\frac{d^2\sigma}{d\Omega dE}\right)_{\alpha,q} \propto (u_q + \sqrt{\sigma}v_q)^2 \tag{31}$$

$$\left(\frac{d^2\sigma}{d\Omega dE}\right)_{\beta,q} \propto (\sqrt{\sigma}u_q + v_q)^2 \tag{32}$$

where, for simplicity, we ignored the differences between Debye-Waller factors and atomic form factors of Ni and Ir [15]. A precise calculation of the cross sections should take these differences into account and is beyond the scope of this study. Nevertheless, from these equations it is evident that the relative intensity difference between the two magnon branches depends strongly on the relative signs of u and v, which in turn depend on the relative signs of $J_{\parallel}$ and $J_{\perp}$. So far, the only neutron scattering study on this compound [17] could not observe the higher energy branch, and as a result there is no data available to compare our prediction with.

TIGHT BINDING MODEL

In order to figure out the important Hamiltonian matrix elements that correspond to dominant hopings between the Ir and Ni ions, we performed a Wannier function calculation to extract a tight binding model. For simplicity, we performed the first principles DFT calculation at this step without the +U correction and with no spin orbit coupling. This gives a simple tight binding model that can be used as a qualitative guide for determining the sign of the superexchange interactions.

We considered the isolated group of bands near the Fermi level that spans a 2.5 eV range and has 16 bands in it. These 16 bands come from the t_{2g} orbitals on Ir and all 5 d orbitals of the Ni ion. The resultant wannier functions are well localized on the ions and has a maximum Im/Re ratio of less than $1.5 \cdot 10^{-3}$. In Fig. 3 we show some examples of the Wannier functions we obtained. Both the Ni and Ir Wannier orbitals have d character, with the Ir ones having significantly larger spread (3.59 Å^2, compared to 1.85 Å^2) and stronger hybridization with the Oxygen anions as expected.

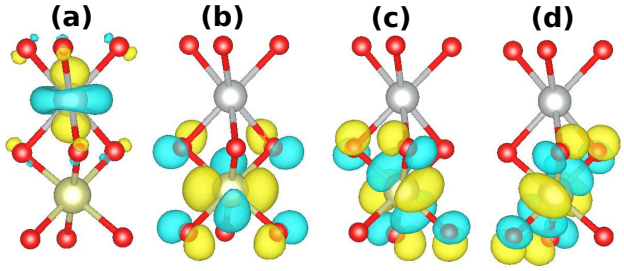

FIG. 3. Some examples of the Wannier functions calculated for the d bands in Sr3NiIrO6. The golden, silver, and red atoms are Ir, Ni, and O respectively. (a) The $|A\rangle$ orbital like function on Ni. (b-d) The three Ir Wannier functions, an almost equal superposition of which give the $|A\rangle$ orbital of Ir.

Using the outcome of the Wannier calculation, the 8×8 Hamiltonian matrix for a nearest neighbor Ni-Ir pair can

be written as

$$\mathcal{H} = \begin{pmatrix} 3.49 & 0 & 0 & 0 & 0 & 0 & 0 & 0.35 \\ 0 & 4.05 & 0 & 0 & 0 & 0 & 0.16 & 0 \\ 0 & 0 & 4.05 & 0 & 0 & 0.16 & 0 & 0 \\ 0 & 0 & 0 & 4.47 & 0 & 0.23 & 0.13 & 0 \\ 0 & 0 & 0 & 0 & 4.47 & 0.13 & -0.23 & 0 \\ 0 & 0 & 0.16 & 0.23 & 0.13 & 4.03 & 0 & 0 \\ 0 & 0.16 & 0 & 0.13 & -0.23 & 0 & 4.03 & 0 \\ 0.35 & 0 & 0 & 0 & 0 & 0 & 0 & 4.18 \end{pmatrix} \quad (33)$$

in a basis that diagonalizes the local atomic hamiltonians. (For simplicity, we set any matrix element that is smaller than 0.03 to zero.) In our notation, the first five components are for the Ni orbitals, and the last three are for Ir orbitals. The diagonal elements of this matrix correctly gives the crystal field splittings for the local atomic environments: The Ni d-orbitals are split $1+2+2$, and the lowest lying, singlet orbital(at 3.49 eV) is the $|3z^2-r^2\rangle$-like orbital shown in Fig. 3a (with 2% mixing with other orbitals). The singlet Ir orbital (at 4.18 eV) is an almost equal superposition of the three Ir Wannier functions shown in Fig. 3b-d, and so it is also $|3z^2-r^2\rangle$-like, as expected from the Ir's trigonal site symmetry and the DFT DOS shown in the main text.

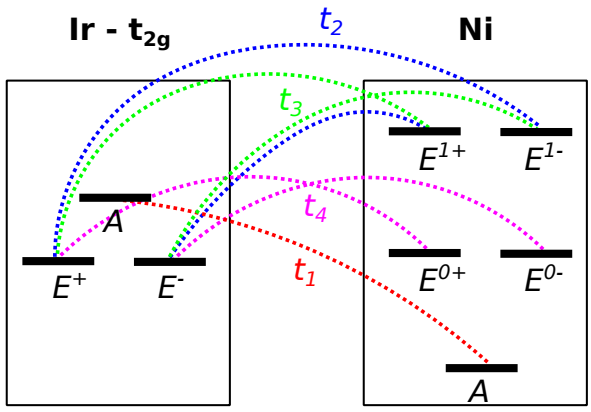

FIG. 4. The nonzero Hamiltonian matrix elements between a nearest neighbor pair of Ir and Ni ions.

In Fig. 4 and Table II, we sketch the inter-atomic Hamiltonian elements. The largest hopping t_1 is between the singlet ($|A\rangle$) orbitals on each atom. This is in line with the expectation that in face-sharing polyhedral geometries, there is usually large direct cation - cation interactions. This is because *(i)* in the face-sharing geometry the Ni and Ir are closer to each other than in other (corner or edge sharing) geometries, so their d orbitals can overlap (which increases direct d-d hopping t_d) [10], and *(ii)* the Ni-O-Ir angle is very far from 180°, so there is not a single oxygen p orbital that is extended towards both the cations (which decreases the oxygen mediated d-O-d hopping t_O). There is also considerable hopping (t_2 and t_3) between the Ir doublet orbitals ($E^{\mp}$) and both of the lower lying, occupied Ni doublet orbitals ($E^{1\mp}$). Finally, there is also a significant hopping element (t_4) between the Ir doublet and the higher lying, partially occupied Ni doublet ($E^{0\mp}$), however, each Ir $E^{\mp}$ has nonzero hopping to only one of the Ni $E^{0\mp}$. Depending on the magnitude of the Hubbard U on either atom as well, each of these hopping elements will give rise to magnetic interactions of different strengths. It is possible to estimate the signs of different terms using the fact that superexchange between partially filled orbitals is AFM (since excitation of one electron from one atom to the other is possible only if the spins are antiparallel), whereas the superexchange between a fully occupied and a partially occupied orbital is ferromagnetic (due to the energy gain via the intra-atomic Hund's coupling in the fully occupied orbital's ion). In the magnetic DFT+U calculation, all Ir t_{2g} orbitals have 1/3 of a hole, the A and $E^{0\mp}$ orbitals Ni are fully occupied, and the $E^{1\mp}$ of Ni are half-occupied. As a result, the t_1 and t_4 lead to a ferromagnetic coupling between total Ni spin and the spins of the A and $E^{\mp}$ orbitals respectively of Ir; and t_2 and t_3 lead to an antiferromagnetic coupling between the Ni spin moment and the spins on the $E^{\mp}$ orbitals on Ir.

The spin-orbit coupling of the Ir ion creates a spin-orbital configuration where the different orbitals have opposite spins. In the magnetic ground state, where the magnetic moments of either ion as well as the spin expectation values are along the z axis (parallel to the chain direction), the Ir $|A\rangle$ orbital has opposite spin to the Ir $|E^{\mp}\rangle$, as shown in Figs. 6 and 7. In this configuration, the superexchange processes due to t_1 anti-aligns the spins of Ni ion and the Ir $|A\rangle$ orbital, and hence leads to an antiferromagnetic/ferrimagnetic coupling between the two ions. t_2 and t_3 also favor anti-parallel alignment of the Ir and Ni pseudo-spins, and the combination of these three terms dominate and results in the intra-chain ferrimagnetic configuration observed in this compound. However, the sign of this coupling changes when we consider a configuration when the magnetic moments are aligned in the x-y plane (perpendicular to the chain directions). In this configuration, the electron in the $J_{\rm eff}=1/2$ orbitals will be in a state $|J_{1/2},\uparrow_x\rangle$ where its magnetic moment is parallel to the x axis. In terms of the $J_{\rm eff}=1/2$ states with moments along $\mp z$, this state can be written as in Eq. 3 of the main text:

$$|J_{1/2},\uparrow_x\rangle = \Big(i\gamma\sqrt{2}|A,\uparrow_x\rangle + |E^+,\uparrow_x\rangle + |E^-,\uparrow_x\rangle + |E^+,\downarrow_x\rangle - |E^-,\downarrow_x\rangle\Big)/\sqrt{2(|\gamma|^2+2)} \quad (34)$$

Note that in our notation, the arrows without subscript refer to (pseudo-)spin directions along the z axis, so $|\uparrow_x\rangle = |\uparrow\rangle + |\downarrow\rangle)/\sqrt{2}$, etc. The spin configuration of the Ir orbitals are different in $|J_{1/2},\uparrow_x\rangle$ than they are in $|J_{1/2},\uparrow\rangle$, and as a result, the superexchange processes that the hoppings t_{1-4} give rise to change sign. Most importantly, the $|A\rangle$ orbital on the Ir ion now has the same

	Ir orbital	Ni orbital	Coupling between spins of orbitals	Coupling between total pseudo-spins (z)
$t_1 = 0.35$	$\|A\rangle$	$\|A\rangle$	FM	AFM
$t_2 = 0.23$	$\|E^{\mp}\rangle$	$\|E^{1\mp}\rangle$	AFM	AFM
$t_3 = 0.13$	$\|E^{\mp}\rangle$	$\|E^{1\pm}\rangle$	AFM	AFM
$t_4 = 0.16$	$\|E^{\mp}\rangle$	$\|E^{0\pm}\rangle$	FM	FM

TABLE II. The hopping amplitudes, the orbitals that they involve on each atom, and the sign of the superexchange that they give rise to. A FM coupling between the $|A\rangle$ orbital on the Ir and the Ni magnetic moment effectively is an antiferromagnetic coupling between the two atoms if the total magnetic moment of the Ir ion is along the z axis.

spin direction as the total Ir moment, and as a result, the superexchange process that t_1 gives rise to couples the Ir and Ni moments ferromagnetically. The other hoppings t_{2-4} are less important when the magnetic moments are along the x direction since the Ir $|E^{\pm}\rangle$ orbitals do not have a spin moment along this direction. The result is a ferromagnetic coupling when the magnetic moments are in the x direction, which explains the sign of the $J_\perp$ term in the main text.

U DEPENDENCE OF MAGNETIC INTERACTIONS

In order to show that the choice of the U parameters used in DFT+U calculations does not introduce a qualitative error in the results presented in this manuscript, in Table III we report values of the anisotropic exchange coupling between nearest neighbor Ni and Ir ions for different values of U on Ni and Ir ions. The strength of the magnetic interactions depend sensitively on the choice of U, as expected. However, for all values of of U's we tested, the main point of this study that the nearest neighbor exchange interaction is radically anisotropic (the signs of $J_\perp$ and $J_\parallel$ are opposite to each other) remains valid.

U	$J_\parallel$ (meV)	$J_\perp$ (meV)
$U_{\rm Ni} = 5$ eV $U_{\rm Ir} = 2$ eV	15.0	-6.3
$U_{\rm Ni} = 5$ eV $U_{\rm Ir} = 1$ eV	16.9	-6.4
$U_{\rm Ni} = 4$ eV $U_{\rm Ir} = 2$ eV	19.0	-8.4
$U_{\rm Ni} = 4$ eV $U_{\rm Ir} = 1$ eV	24.1	-10.8
$U_{\rm Ni} = 3$ eV $U_{\rm Ir} = 1$ eV	37.4	-18.4
$U_{\rm Ni} = 2$ eV $U_{\rm Ir} = 1$ eV	26.3	-2.6

TABLE III. The values of $J_\parallel$ and $J_\perp$ for different values of Hubbard U on Ni and Ir ions.

SINGLE ION ANISOTROPY

As discussed in the main text, an anisotropic exchange model with additional strong single ion anisotropy (SIA) on the Ni ion was used to explain the magnon spectrum of Sr_3NiIrO_6 in Ref. [16]. The Ni^{2+} cation in Sr_3NiIrO_6 has its d orbitals split into 1+2+2, and has 2 holes on the higher energy doublet. This configuration leads to a quenched orbital angular momentum. On the other hand, the crystal field splitting of Ni is not very large (a fact that is usually valid for trigonal prismatic coordination environments, but can also be deduced from the Wannier model), and hence this quenching cannot be very strong. As a result, even though we don't expect SIA to be the dominant source of anisotropy, we cannot preclude that it has a measurable effect.

In this section, we fit different models to the data reported in Fig. 4 of the main text, to show that a model with SIA can also explain the energy values for different magnetic configurations, obtained from first principles calculations. We consider three models:

- Model I: Anisotropic exchange without SIA. (Fig. 5a) This is the *minimal* model that we used in the main text.
- Model II: Isotropic exchange with SIA on Ni. (Fig. 5b) This model considers the interaction between Ni and Ir to be ordinary Heisenberg type ($\sim \vec{S}_i \cdot \vec{S}_j$). This model has the same number of parameters as Model I.
- Model III: Anistropic exchange with SIA on Ni. (Fig. 5c) This is the most general model that takes into account both the interaction and the SIA on Ni as sources of anisotropy.

Within the error bars of DFT, all of these three models provide fits to the data of comparable quality. The best fit is obtained by model III, which has the largest number of fitted parameters. As a result, the energy values we obtain from DFT alone are not sufficient to conclusively differentiate between different models and say that the SIA does not have a considerable effect.

The character of the magnetic configurations we could stabilize in DFT, on the other hand, strongly suggests the presence of a radically anisotropic exchange. We could

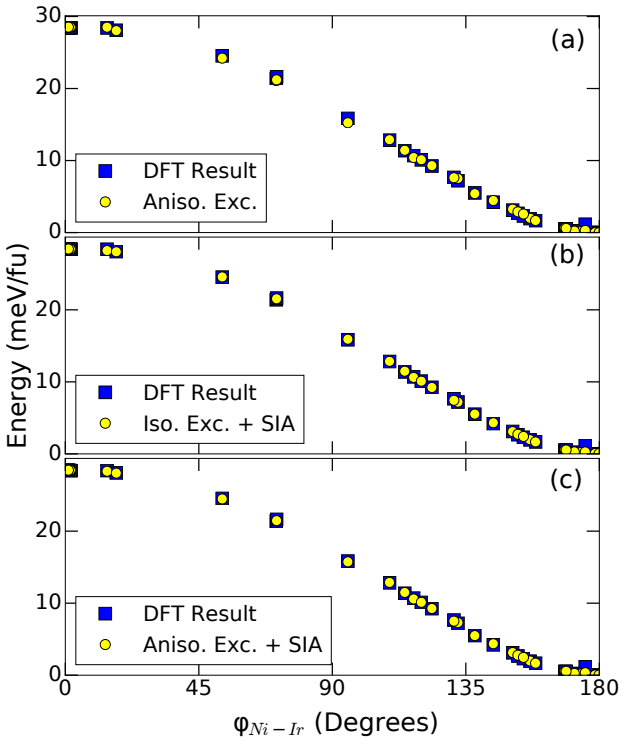

FIG. 5. Energy as a function of the angle between the magnetic moments of nearest-neighbor atoms, as obtained from first principles calculations, and different models fitted to the first principles data. (a) Model I, anisotropic exchange (same as in the main text). (b) Model II, isotropic exchange with SIA on the Ni ion, (c) Model III, anisotropic exchange with SIA on the Ni ion.

only stabilize states with (i) anti-parallel magnetic moment components along the c axis, and (ii) parallel magnetic moment components on the ab plane. We could not stabilize the ferrimagnetic state with anti-parallel moments in the ab plane. This is the reason that in the main text, we use only a model with anisotropic exchange, which is the model with smallest number of parameters that can both reproduce the energy values calculated, and explain the particular magnetic states that could be stabilized.

Obtaining both the magnitude of anisotropic exchange and SIA was unfortunately not possible, because the magnetic configurations we could stabilize, which had $90° - \phi_{\rm Ni} \approx \phi_{\rm Ir} - 90°$ (Fig. 4b of main text), render a model with both anisotropic exchange and SIA underdetermined, and it is not possible to find a unique fit. For example, even though the fitted data looks almost identical in Fig. 5 b and c for models I and II, the magnitudes of the SIA terms for them are quite different; 2.0 meV and 1.4 meV respectively. The difference between the $J_{\parallel}$ values from model I and III are even more different; 19.5 meV and 9.3 meV respectively. A more advanced first principles method that either utilizes constrained magnetic moments [18] or Green's functions approaches [19] is required to be able to extract the magnitude of the SIA in this compound.

[1] G. Kresse and J. Furthmuller, "Efficiency of ab-initio total energy calculations for metals and semiconductors using a plane-wave basis set," Computational Materials Science **6**, 15–50 (1996).

[2] G. Kresse and J. Furthmüller, "Efficient iterative schemes for *ab initio* total-energy calculations using a plane-wave basis set," Phys. Rev. B **54**, 11169–11186 (1996).

[3] P. E. Blöchl, "Projector augmented-wave method," Phys. Rev. B **50**, 17953–17979 (1994).

[4] G. Kresse and D. Joubert, "From ultrasoft pseudopotentials to the projector augmented-wave method," Phys. Rev. B **59**, 1758–1775 (1999).

[5] John P. Perdew, Adrienn Ruzsinszky, Gábor I. Csonka, Oleg A. Vydrov, Gustavo E. Scuseria, Lucian A. Constantin, Xiaolan Zhou, and Kieron Burke, "Restoring the density-gradient expansion for exchange in solids and surfaces," Phys. Rev. Lett. **100**, 136406 (2008).

[6] S. L. Dudarev, G. A. Botton, S. Y. Savrasov, C. J. Humphreys, and A. P. Sutton, "Electron-energy-loss spectra and the structural stability of nickel oxide: an LSda+u study," Phys. Rev. B **57**, 1505–1509 (1998).

[7] E. Lefrançois, L. C. Chapon, V. Simonet, P. Lejay, D. Khalyavin, S. Rayaprol, E. V. Sampathkumaran, R. Ballou, and D. T. Adroja, "Magnetic order in the frustrated ising-like chain compound Sr_3NiIrO_6," Phys. Rev. B **90**, 014408 (2014).

[8] Günter Bergerhoff and O Schmitz-Dumont, "Die kristallstruktur des kaliumhexachlorocadmats (ii)," Zeitschrift für anorganische und allgemeine Chemie **284**, 10–19 (1956).

[9] TN Nguyen and H-C Zur Loye, "A family of one-dimensional oxides: Sr_3MIrO_6 (M= Ni, Cu, Zn): Structure and magnetic properties," Journal of Solid State Chemistry **117**, 300–308 (1995).

[10] J.B. Goodenough, *Magnetism and the chemical bond*, Interscience monographs on chemistry: Inorganic chemistry section (Interscience Publishers, 1963).

[11] Roald Hoffmann, James M Howell, and Angelo R Rossi, "Bicapped tetrahedral, trigonal prismatic, and octahedral alternatives in main and transition group six-coordination," Journal of the American Chemical Society **98**, 2484–2492 (1976).

[12] Grigori V Vajenine, Roald Hoffmann, and Hans-Conrad zur Loye, "The electronic structures and magnetic properties of one-dimensional ABO_6 chains in Sr_3ABO_6 (A= Co, Ni; B= Pt, Ir) and two-dimensional MO_3 sheets in $InMO_3$ (M= Fe, Mn)," Chemical physics **204**, 469–478 (1996).

[13] MI Aroyo, JM Perez-Mato, C Capillas, E Kroumova, S Ivantchev, G Madariaga, A Kirov, and H Wondratschek, "Bilbao crystallographic server: I. databases and crystallographic computing programs," Zeitschrift fur Kristallographie **221**, 15–27 (2006).

[14] Patrick Fazekas, *Lecture notes on electron correlation and magnetism*, Vol. 5 (World scientific, 1999).

[15] S.W. Lovesey, *Theory of Neutron Scattering from Con-*

densed Matter, International Series of Monogr No. 2. c. (Clarendon Press, 1986).

[16] E. Lefrançois, A.-M. Pradipto, M. Moretti Sala, L. C. Chapon, V. Simonet, S. Picozzi, P. Lejay, S. Petit, and R. Ballou, "Anisotropic interactions opposing magnetocrystalline anisotropy in Sr_3NiIrO_6," Phys. Rev. B **93**, 224401 (2016).

[17] S. Toth, W. Wu, D. T. Adroja, S. Rayaprol, and E. V. Sampathkumaran, "Frustrated ising chains on the triangular lattice in Sr_3NiIrO_6," Phys. Rev. B **93**, 174422 (2016).

[18] Peitao Liu, Sergii Khmelevskyi, Bongjae Kim, Martijn Marsman, Dianzhong Li, Xing-Qiu Chen, D. D. Sarma, Georg Kresse, and Cesare Franchini, "Anisotropic magnetic couplings and structure-driven canted to collinear transitions in sr_2iro_4 by magnetically constrained noncollinear dft," Phys. Rev. B **92**, 054428 (2015).

[19] Igor Solovyev, Noriaki Hamada, and Kiyoyuki Terakura, "Crucial role of the lattice distortion in the magnetism of $lamno_3$," Phys. Rev. Lett. **76**, 4825–4828 (1996).